

Extremely red Kuiper-belt objects in near-circular orbits beyond 40 AU

S. C. Tegler* & W. Romanishin†

* Department of Physics & Astronomy, Northern Arizona University, Flagstaff, Arizona 86011, USA

† Department of Physics & Astronomy, University of Oklahoma, Norman, Oklahoma 73019, USA

Kuiper-belt objects (KBOs) are an ancient reservoir of comets beyond Neptune's orbit^{1,2}. Some of these objects were recently found to have the reddest optical colours in the Solar System³, but the number of objects for which accurate colours were available was too small for any correlation to be discerned between colour and physical or dynamical properties, which might shed light on the origin of these objects. Here we report that all nine of the KBOs in our survey on near-circular (low-eccentricity) orbits with perihelion distances larger than 40 AU have extremely red surfaces, thereby connecting an observable property with a dynamical class. Of the objects with orbital eccentricities greater than 0.1, about half are also very red, while the rest have colours similar to the Sun, meaning that reflected sunlight is not strongly modified by the objects' surface properties. In addition, of the 13 'classical' KBOs (those with semimajor axis $a \approx 45$ AU and eccentricity $e < 0.15$), the ten that are very red are in orbits with small angles of inclination to the ecliptic, whereas the three with solar colours are all in high-inclination orbits. We suggest that these three 'grey' classical KBOs may be part of a dynamical group that is separate from the 'red' classical KBOs.

Our survey uses the low-resolution imaging spectrometer (LRIS), B (438 nm), V (547 nm), and R (642 nm) glass filters, and a $2,048 \times 2,048$ CCD (charge coupled device) at the $f/15$ Cassegrain focus of the 10-m Keck II telescope⁴. Each of our images covers 6×7 arcmin on the sky at 0.21 arcsec per pixel and has a stellar point-spread function full-width at half-maximum of about 0.7 arcsec. We correct instrumental magnitudes to zero air mass using nightly extinction coefficients and place them on the Kron-Cousins system using transformation equations from observations of Landolt standard star fields⁵. A full description of our data reduction and analysis techniques can be found in the literature^{3,6-8}.

Table 1 presents our results. Measurements for 17 objects come from the Keck telescope, and measurements for four objects come

from the 1.8-m Vatican telescope and the 2.3-m University of Arizona telescope. In Fig. 1a, we plot 17 points from observations on the Keck telescope, two points from observations on the Vatican telescope, and 13 points from our original survey on the University of Arizona 2.3-m telescope³. Colours for KBOs and Centaurs (recent refugees from the Kuiper belt on outer planet-crossing orbits) are represented by filled and open squares, respectively. The colour of the Sun is represented by the standard solar symbol at $B - V = 0.67$ and $V - R = 0.36$. The reddest objects are toward the upper right-hand corner of Fig. 1a. The impact of the new data on our survey can be seen in the $B - R$ histogram in Fig. 1b. We obtain the $B - R$ colour for a KBO from the sum of the $B - V$ and $V - R$ colours. The Sun has a $B - R$ colour of 1.03. The reddest objects in Fig. 1b are in bins with the largest values of $B - R$. Values from our original survey and the current survey are represented by grey and white bars, respectively. Despite a spread in colour space by the current survey, we clearly see a double-peaked distribution in the $B - R$ histogram. Apparently, the surfaces of some KBOs and Centaurs are rich in a material that absorbs blue sunlight. The lack of blue light upon reflection gives the surfaces their red colour. Other KBOs and Centaurs have little or none of the blue absorber. The material on their surfaces absorbs blue, yellow and red sunlight with a similar efficiency and we refer to the surfaces of these objects as grey in colour.

Now that our survey has a significant number of KBOs and Centaurs, we can look for patterns between the colours of the objects and their orbital elements. In Fig. 2a, we plot $B - R$ colour against perihelion distance, q . The Centaurs (open squares) and KBOs (filled squares) are evenly split between red surfaces (top) and grey surfaces (bottom) for perihelion distances between 6 and 40 AU. Beyond 40 AU, all seven KBOs with $B - R$ colours reside in the red group. In addition to the seven KBOs with known $B - R$ colours, there are two more KBOs in Table 1 with perihelion distances beyond 40 AU that are in the red group only on the basis of their $V - R$ colours: these are 1997 CU29 and 1997 CT29. A statistical calculation suggests the probability of getting the first nine objects with perihelion distances greater than 40 AU all red in a population that is evenly split between red and grey colours (as it is for perihelion distances out to 40 AU) is 1 in 512. Evidently, KBOs with perihelion distances greater than 40 AU are dominated by extraordinarily red surfaces.

There is another possible pattern in Fig. 2a. Objects in the red group appear redder with smaller perihelion distance. Perhaps we are seeing the effect of an increase of solar radiation modifying the surfaces.

Table 1 Keck colours of Kuiper-belt objects and Centaurs

Object	Class	V	$\frac{\sigma}{\sqrt{n}}$	B - V	$\frac{\sigma}{\sqrt{n}}$	V - R	$\frac{\sigma}{\sqrt{n}}$	UT
1999 TR11	Plutino	23.51	0.07	1.02	0.08	0.75	0.07	1999 Oct 07
1999 OY3	Classical	22.53	0.02	0.71	0.01	0.37	0.02	1999 Sep 08
1998 WX24	Classical	23.44	0.04	1.09	0.05	0.70	0.05	1999 Oct 07
1998 WV24	Plutino	23.41	0.01	0.77	0.01	0.50	0.03	1999 Sep 08
1998 WH24*	Classical	21.23	0.01	0.94	0.03	0.62	0.03	1999 Nov 08-12
1998 SM165*	1:2	21.61	0.05	1.01	0.10	0.75	0.07	1999 Nov 13-15
1997 SZ10	1:2	23.69	0.03	1.14	0.08	0.65	0.03	1999 Oct 07
1997 QH4	Classical	23.70	0.04	1.01	0.07	0.67	0.05	1998 Oct 26
1997 CU29†	Classical	23.31	0.08			0.66	0.04	1998 Jan 23-26
1997 CT29†	Classical	23.72	0.11			0.75	0.12	1998 Jan 23-26
1996 TK66	Classical	23.14	0.03	0.99	0.02	0.63	0.02	1998 Oct 26
1996 SZ4	Plutino	23.33	0.03	0.83	0.03	0.52	0.02	1999 Sep 07
1996 RR20	Plutino	23.57	0.01	1.16	0.04	0.71	0.03	1999 Sep 07
1995 QZ9	Plutino	24.12	0.02	0.88	0.04	0.52	0.03	1999 Sep 07
1994 VK8	Classical	24.07	0.05	1.01	0.06	0.67	0.03	1998 Oct 26
1993 SB	Plutino	23.13	0.01	0.82	0.03	0.47	0.04	1999 Sep 08
1993 RO	Plutino	23.95	0.03	0.85	0.07	0.51	0.06	1999 Sep 08
1992 QB1	Classical	23.79	0.03	0.92	0.06	0.78	0.03	1999 Sep 08
1999 OX3	Centaur	22.45	0.03	1.12	0.03	0.69	0.01	1999 Sep 08
1998 QM107	Centaur	23.11	0.02	0.73	0.02	0.52	0.03	1999 Sep 07
1994 TA	Centaur	24.31	0.05	1.24	0.10	0.68	0.03	1998 Oct 26

* Vatican Observatory 1.8-m.

† University of Arizona 2.3-m.

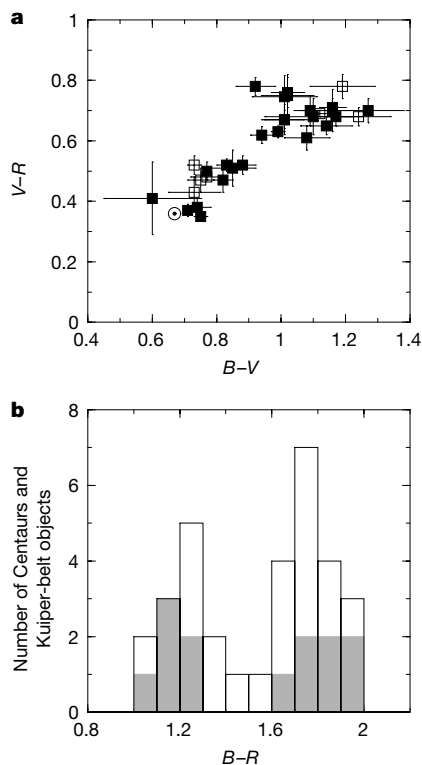


Figure 1 Surface colours of KBOs. **a**, A colour–colour plot of the KBOs (solid squares) and Centaurs (open squares) in our survey. The colour of the Sun is represented by the standard solar symbol at $B - V = 0.67$ and $V - R = 0.36$. The error bars are the uncertainty in the mean, σ/\sqrt{n} , where σ is the standard deviation of n 300-second exposures. Photon noise, sky noise, and ‘unseen’ background objects just below our detection limit are sources of random error that contribute to the size of the error bars. Thirteen points come from our initial survey³, seventeen points come from recent observations on the 10-m Keck telescope, and two points come from recent observations on the 1.8-m Vatican telescope. The reddest objects are toward the upper right-hand corner. **b**, A $B - R$ histogram of the 32 objects in our survey that comes from the sum of their $B - V$ and $V - R$ colours. The grey and white bars represent our initial and current surveys, respectively. The reddest objects are in bins with the largest values of $B - R$. There is a clear double-peaked distribution of colours.

Besides patterns in perihelion distance, we can see some important trends in a plot of eccentricity, e , against semimajor axis, a . In Fig. 2b, we see that our survey contains 13 KBOs, Plutinos, on stable Pluto-like orbits in a 2:3 resonance with Neptune ($a \approx 39.5$ AU and $0.1 < e < 0.3$) and 13 classical KBOs on distant and near-circular orbits ($a \approx 45$ AU and $e < 0.15$). Objects with perihelion distances at and beyond 40 AU fall on and below the curve toward the lower right-hand corner of Fig. 2b. In our survey we find four red and four grey Centaurs, six red and seven grey Plutinos, and ten red and three grey classical KBOs. Unlike the Centaurs and Plutinos which are evenly split between red and grey colours, the classical KBOs are dominated by red colours. The dominance of red surfaces among the classical KBOs is due to the nine KBOs with perihelion distances greater than 40 AU.

The ten classical KBOs with red colours share a trait that the three classical KBOs with grey colours do not share. In particular, the ten red objects are all on orbits with small inclination angles to the ecliptic, less than 13° . On the other hand, the three grey objects are all on orbits with large inclination angles, greater than 24° . The probability of getting ten classical KBOs with the lowest inclination orbits all red in a population that is evenly split between red and grey colours is 1 in 1,024. Perhaps the three high-inclination grey KBOs currently classified as classical KBOs are really members of a separate dynamical group.

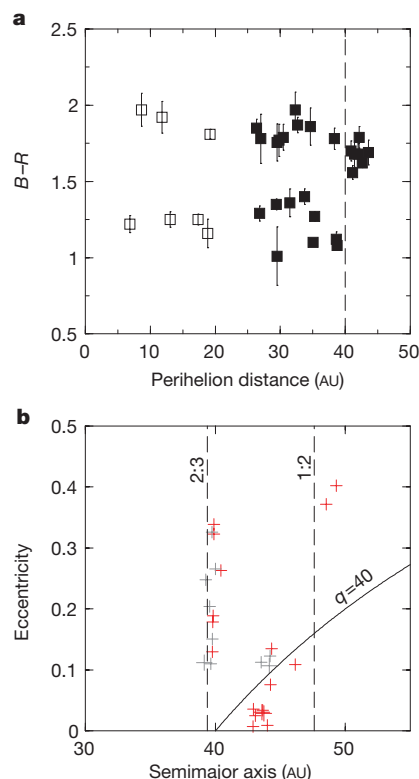


Figure 2 Objects on circular orbits beyond 40 AU are red. **a**, A plot of $B - R$ colour against perihelion distance for the objects in our survey. The uncertainties in q are smaller than the size of the symbols. The objects with perihelion distances between 6 and 40 AU are evenly split between the red (larger $B - R$ values) and grey (smaller $B - R$ values) groups, but all seven KBOs with perihelion distances beyond 40 AU and $B - R$ colours are red. **b**, A plot of orbital eccentricity against semimajor axis. Red and grey symbols represent objects with red and grey surface colours, respectively. Although the Plutinos ($a \approx 39.5$ AU) are evenly split between the red and grey groups, the classical KBOs ($a \approx 45$ AU) are dominated by red surface colours. All nine classical KBOs in our survey with perihelion distances greater than 40 AU, below the curve toward the lower right-hand side of the figure, are red.

Another noteworthy point concerns the two red KBOs in the 1:2 resonance with Neptune in Fig. 2b ($a \approx 48$ AU and $e \approx 0.4$). KBOs that are currently in the 2:3 and 1:2 resonances with Neptune may initially have been on circular orbits closer to the Sun, but as Neptune migrated outward, it swept them outward onto eccentric orbits⁹. Perhaps the two objects in the 1:2 resonance in Fig. 2b were initially on near-circular orbits among the classical KBOs with red surface colours. □

Received 24 July; accepted 11 September 2000.

- Jewitt, D. & Luu, J. Discovery of the candidate Kuiper belt object 1992 QB1. *Nature* **362**, 730–732 (1993).
- Marsden, B. G. List of transneptunian objects. (Cited June 2000) <<http://cfa-www.harvard.edu/cfa/pubs/lists/TNOs.html>> (2000).
- Tegler, S. C. & Romanishin, W. Two distinct populations of Kuiper-belt objects. *Nature* **392**, 49–51 (1998).
- Oke, J. B. *et al.* The Keck Low Resolution Imaging Spectrometer. *Publ. Astron. Soc. Pacif.* **107**, 375–385 (1995).
- Landolt, A. U. UBVR photometric standard stars in the magnitude range $11.5 < V < 16.0$ around the celestial equator. *Astron. J.* **104**, 340–371 (1992).
- Romanishin, W., Tegler, S. C., Levine, J. & Butler, N. BVR photometry of centaur objects 1995 GO, 1993 HA2, and 5145 Pholus. *Astron. J.* **113**, 1893–1898 (1997).
- Tegler, S. C. & Romanishin, W. The extraordinary colors of trans-neptunian objects 1994 TB and 1993 SC. *Icarus* **126**, 212–217 (1997).
- Tegler, S. C., Romanishin, W., Stone, A., Tryka, K., Fink, U. & Fevig, R. Photometry of the trans-neptunian object 1993 SC. *Astron. J.* **114**, 1230–1233 (1997).
- Malhotra, R. The origin of Pluto’s orbit: implications for the solar system beyond Neptune. *Astron. J.* **110**, 420–429 (1995).

Acknowledgements

We thank the NASA Planetary Astronomy programme for financial support of this research and the NASA Keck Telescope Allocation Committee for consistent allocation of telescope time.

Correspondence and requests for materials should be addressed to S.C.T. (e-mail: tegler@proto.phy.nau.edu).

n-type colloidal semiconductor nanocrystals

Moonsub Shim & Philippe Guyot-Sionnest

James Franck Institute, University of Chicago, 5640 S. Ellis Avenue, Chicago, Illinois 60637, USA

Colloidal semiconductor nanocrystals^{1,2} combine the physical and chemical properties of molecules with the optoelectronic properties of semiconductors. Their colour is highly controllable, a direct consequence of quantum confinement on the electronic states³. Such nanocrystals are a form of ‘artificial atoms’ (ref. 4) that may find applications in optoelectronic systems such as light-emitting diodes^{5,6} and photovoltaic cells⁷, or as components of future nanoelectronic devices. The ability to control the electron occupation (especially in n-type or p-type nanocrystals) is important for tailoring the electrical and optical properties, and should lead to a wider range of practical devices. But conventional doping by introducing impurity atoms has been unsuccessful so far: impurities tend to be expelled from the small crystalline cores (as observed for magnetic impurities⁸), and thermal ionization of the impurities (which provides free carriers) is hindered by strong confinement. Here we report the fabrication of n-type nanocrystals using an electron transfer approach commonly employed in the field of conducting organic polymers⁹. We find that semiconductor nanocrystals prepared as colloids can be made n-type, with electrons in quantum confined states.

Electron transfer in and out of nanocrystals has been a subject of study for many years, mostly in the context of photochemistry and photovoltaics¹⁰. However, there has never been any conclusive evidence that injected electrons could be placed in the Lowest Unoccupied Quantum-Confined Orbital (we will use the acronym LUQCO) which is the essence of making n-type nanocrystals. Instead, the electrons were most probably transferred to trap states. Reducing the nanocrystals such that they are n-type requires the absence or saturation of electron traps and a slow kinetics towards oxidation. This may seem hopeless given the large surface area of the nanocrystals and the possible presence of many dangling bonds. However, the conduction band minimum of many semiconductors lies near the reduction potential of hydrogen¹¹, well below the reduction potential of alkali metals (for example, the reduction potential of Na = -2.71 V versus SHE). While quantum confinement shifts the energy levels of the conduction band higher (relative to the bulk), that shift is typically less than 1 eV for most sizes of quantum dots studied. Therefore it should be feasible to inject electrons into semiconductor nanocrystals with alkali metals in a manner similar to organic polymers⁹, C₆₀ (ref. 12) and carbon nanotubes¹³. Using surface-passivated nanocrystals in anhydrous and de-aerated solutions, we have observed successful electron transfer from sodium biphenyl to the LUQCO of colloidal semiconductor nanocrystals, making them the first n-type nanocrystals. The radical anion of biphenyl acts as the charge shuttle. The n-type nanocrystals can also be obtained by simply exposing a solution of

nanocrystals to chunks of sodium. However, this process typically takes several days owing to the low mobility of the nanocrystals.

To ascertain that the electrons are successfully placed in the LUQCO of the nanocrystals, rather than merely charging them by occupation of surface states, infrared spectroscopy of the 1S_c-1P_c intraband transition has been used. As seen in the inset of Fig. 1, if an electron is successfully transferred into the LUQCO (labelled 1S_c for a spherical nanocrystal), a strong electronically allowed infrared transition to the next higher state (labelled 1P_c) must appear. At the same time, a bleach of the exciton transition must occur as a result of the occupation of the 1S_c state. Therefore a combination of infrared and optical spectroscopy provides a rigorous diagnosis of the n-type character of the nanocrystals.

In Fig. 1, infrared and visible absorption spectra of 5.2-nm CdSe nanocrystals before (dotted line) and about 1 minute after (solid line) the addition of sodium biphenyl reagent are shown. Upon charge transfer, the first and the second exciton peaks at 2.07 and 2.18 eV, respectively, are strongly bleached and broadened. Broadening is expected if there are charges that can shift the exciton energy by the Stark effect and this can also lead to an apparent blue shift. As the charges may reside in surface states and/or in the delocalized 1S_c state, the changes in the visible absorption indicate that electron transfer may possibly have occurred but do not guarantee that the nanocrystals are n-type. The true n-type character of the nanocrystals is unambiguously confirmed by the appearance of the 1S_c-1P_c infrared absorption arising at 0.3 eV.

The size-dependence of this 1S_c-1P_c transition in the n-type nanocrystals is similar to photoexcited nanocrystals^{14,15}. Figure 2 shows infrared absorption spectra corresponding to the 1S_c-1P_c transition in n-type CdSe nanocrystals of different sizes capped with trioctylphosphine oxide (TOPO). Figure 3 compares the size dependence of the 1S_c-1P_c transition observed in n-type CdSe nanocrystals (filled circles) to the effective mass calculation¹⁶ (solid line) and shows a fair agreement. A previously reported 1S_c-1P_c transition observed in optically excited CdSe nanocrystals¹⁴ (open triangles) as well as for n-type CdSe nanocrystals with various caps (filled diamonds) are also shown in Fig. 3. As we expected, whether

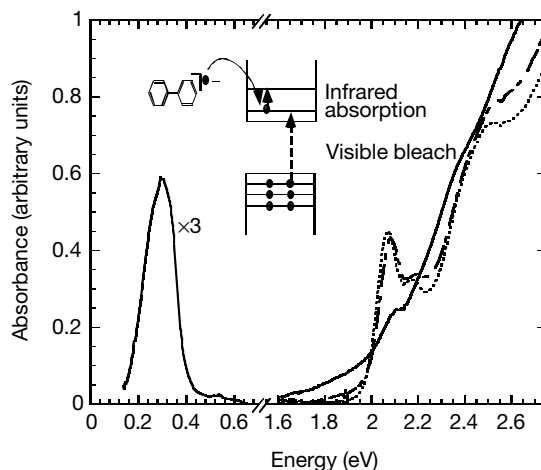


Figure 1 Absorption spectra of CdSe nanocrystals. Spectra are shown before (dotted line), immediately after (solid line), and 27 hours after (dashed line) the addition of sodium biphenyl reagent. The concurrent optical bleach of the first two exciton transitions and the appearance of the infrared absorption are clearly seen. The blue-shift of the optical spectra after the disappearance of the infrared absorption suggests that the n-type nanocrystals decompose by loss of the outermost layer of the semiconductor. Typically, n-type nanocrystals are made by addition of sodium biphenyl to a dried and degassed solution of nanocrystals in heptamethylnonane (~0.1 mM in nanocrystals and ~50 mM in sodium biphenyl). Small amounts of TOPO (<5 mg ml⁻¹) can be added to prevent precipitation.